IARJSET ISSN (O) 2393-8021, ISSN (P) 2394-1588

International Advanced Research Journal in Science, Engineering and Technology

Impact Factor 8.066 ⁜ Peer-reviewed / Refereed journal ⁜ Vol. 12, Issue 2, February 2025

DOI: 10.17148/IARJSET.2025.12240

Single-Stage PV-Grid System to Stabilize DC-link Voltage

Vivek Kushawaha[1]*, Priyesh Kumar Pandey[2]

Department of Electrical Engineering, MG Institute of Management & Technology, Lucknow, India[1]

Department of Electrical Engineering, Ganpat University, Mehsana, Gujarat, India[2]

Abstract: This paper presents a fuzzy logic-based Maximum Power Point Tracking (MPPT) controller for a single-stage solar PV grid-integrated system. The proposed scheme integrates MPPT, grid synchronization, voltage and current regulation, and ripple mitigation to enhance inverter performance. A Fuzzy Logic Controller (FLC) optimizes MPPT for efficient power extraction, while an H-bridge inverter with dual-loop control ensures DC-link voltage stability and unity power factor operation. Simulation results confirm that the inverter output current meets IEEE 519 and IEC 61727 THD standards.

Keywords: Photovoltaic (PV); single-stage; grid-interfaced PV system; FLC MPPT.

1. INTRODUCTION

traditional energy resources like fossil fuels have led to the increasing adoption of renewable energy sources [1-10]. Among various renewable energy sources, solar power gained more popularity due to its pollution-free nature, absence of mechanical moving parts, long lifespan, and silent operation [1, 10-11].

The solar-PV generates DC Power and to integrate this DC power with an AC utility grid, an inverter is needed to transform DC power to AC. Additionally, the non-linear nature of Solar-PV requires a maximum power point tracking (MPPT) device to operate PV at Maximum Power Point (MPP) [12]. The grid-tied PV systems are either a single-stage or two-stage conversion configuration. The two-stage approach involves two distinct conversion steps: (1) a DC-DC converter that manages voltage regulation and MPPT, and (2) an inverter that delivers a sinusoidal current to the grid. While, the single-stage approach integrates both MPPT and grid synchronization within a single DC-AC inverter, leading to a more efficient system design [13].

The dual-stage conversion approach has certain limitations, including higher costs, lower efficiency, and a larger system. To overcome these drawbacks, researchers propose single-stage grid-connected system: A. Alenezi and H. A. Hussain [14] proposed an inverter topology with MPPT, enhancing PV array voltage and converting DC power into AC for grid integration, reducing conversion losses and improving performance. F. E. Aamri et al. [15] introduced a transformerless single-stage PV system, eliminating the transformer to cut costs, weight, and complexity while efficiently interfacing with the grid and minimizing power losses. K. Alluhaybi et al. [16] surveyed single-phase grid-connected inverters for PV systems, evaluating various topologies based on lifetime, efficiency, and cost, aiding optimal selection. S. K. Kuncham et al. [17] compared power losses in single and two-stage PV arrays, demonstrating that single-stage systems reduce costs and losses despite two-stage systems' control flexibility. Dasgupta et al. [18] proposed a series-connected inverter for microgrids to mitigate voltage issues and enhance power quality. Pardhi et al. [19] developed a high-gain boost converter (HGBC) topologies to enhance power extraction and efficiency in grid-integrated PV systems. To operate PV at MPPT sliding mode control (SMC) is used. Additionally, Fifth-Order Generalized Integrator (FiOGI) grid synchronization techniques are used to improve power quality under grid disturbances.

In the view of above literature survey, this paper explores a single-stage grid-interfaced PV power generation system. This method offers several advantages, such as reduced cost, enhanced simplicity, a more compact design, and improved efficiency. Additionally, the proposed system operated PV at its MPP regardless of variation in solar irradiance during injection of current to the utility grid. Furthermore, the system operates at unity power factor. The fuzzy logic controller (FLC)-based MPPT algorithm [20-22]. The proposed algorithm is fast and tracks MPP precisely, even in dynamically changing atmospheric conditions. To ensure stability and compliance with IEEE 519 standards, the PV inverter is designed to achieve a fast dynamic response and high-power quality. IEEE standards specify that the Total Harmonic Distortion (THD) in grid injected current should not exceed 5% [12-26].

IARJSET ISSN (O) 2393-8021, ISSN (P) 2394-1588

International Advanced Research Journal in Science, Engineering and Technology

Impact Factor 8.066 ⁜ Peer-reviewed / Refereed journal ⁜ Vol. 12, Issue 2, February 2025

DOI: 10.17148/IARJSET.2025.12240

2. METHODOLOGY

Fig. 1 presents a generalized scheme of a grid-connected single-stage PV system. The scheme comprises a PV array, an H-bridge VSI, and a DC link buffer at the input side for voltage regulation (C_{dc}). Additionally, an LCL filter is before the grid connection to attenuate harmonics.

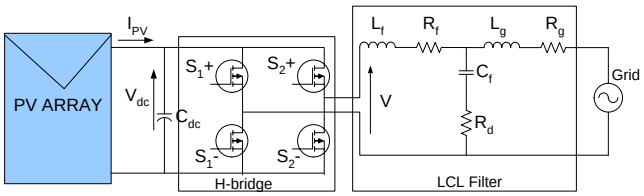

Fig. 1. Grid-interfaced single-stage PV system.

3. CONTROL SCHEME

In the control strategy, an FLC-MPPT controller, a grid synchronization algorithm, a DC link voltage controller, and a current-controlled VSI are used. VSI control scheme ensures that the grid current accurately follows the sinusoidal reference, achieving a quick dynamic response with good power factor, and acceptable THD. The integration of the FLC-based MPPT algorithm enhances the control scheme by automatically regulating the DC link voltage reference and grid power injection. The overall control framework is illustrated in Fig. 2.

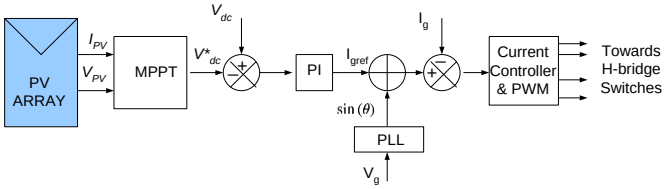

Fig. 2. Control scheme representation

3.1. FLC MPPT ALGORITHM

The PV system exhibits nonlinear voltage-current (I-V) characteristics that vary with atmospheric conditions such as irradiance and temperature. Therefore, an MPPT controller is crucial to operate PV at MPP. Various MPPT techniques have been explored and developed to optimize PV system performance [1, 10-11].

In this paper, an FLC-based MPPT algorithm is employed due to its fast response, ability to control imprecise systems, robustness, and the elimination of the need for an exact mathematical model [21,22]. Moreover, it effectively tracks the MPP with minimal oscillations, even under rapidly changing weather conditions.

Fig. 3 illustrates the schematic diagram of the FLC-based MPPT system. During the fuzzification stage, numerical input and output values are converted into a fuzzy domain with five fuzzy subsets, as shown in Fig. 4. At MPP, the change in input power (ΔP(X)) is zero. Figure 4(b) depicts the variation in PV array current (ΔI(X)), while Fig. 4(c) shows the corresponding change in DC voltage reference (ΔV_dc-ref). The inputs of FLC controller are the change in PV power (ΔP) and the change in PV current (ΔI) at a given sample time (X).

$$\Delta P(X) = P(X) - P(X-1) \qquad (1)$$

TABLE I FUZZY RULE BASE

ΔP \ ΔI	NB	NS	ZE	PS	PB
NB	ZE	ZE	PS	NS	NS
NS	ZE	ZE	ZE	NS	NB
ZE	PB	PS	ZE	NS	NB
PS	PB	PS	ZE	ZE	ZE
PB	PB	PS	NS	ZE	ZE

IARJSET ISSN (O) 2393-8021, ISSN (P) 2394-1588

International Advanced Research Journal in Science, Engineering and Technology

Impact Factor 8.066 ⁜ Peer-reviewed / Refereed journal ⁜ Vol. 12, Issue 2, February 2025

DOI: 10.17148/IARJSET.2025.12240

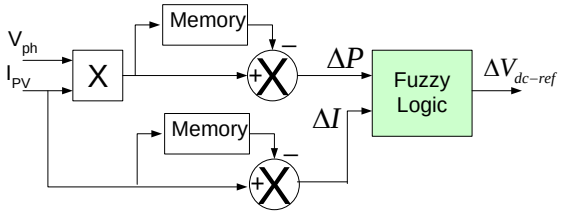

Fig. 3. FLC algorithm Schematic.

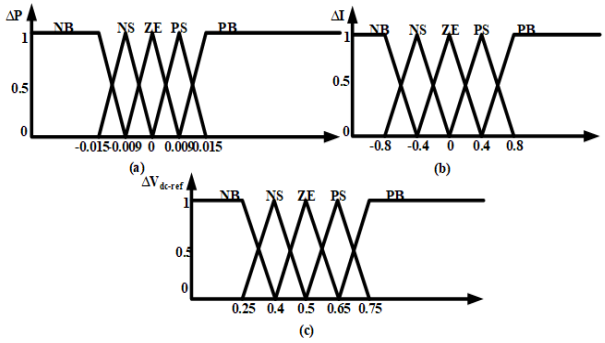

Fig. 4. Membership function of (a) ΔP (b) ΔI (c) $\Delta V_{dc\text{-}ref}$.

$$\Delta I(X) = I(X) - I(X-1) \qquad (2)$$

and fuzzy logic controller output is the DC reference voltage

$$\Delta V_{dc-ref} = V_{dc-ref}(X) - V_{dc-ref}(X-1) \qquad (3)$$

By utilizing these membership functions and dividing the fuzzy subsets appropriately, the computational effort required to determine the control output is significantly reduced, while maintaining minimal steady-state oscillations. Once the input variables, ΔP(X) and ΔI(X), are converted into linguistic variables, the corresponding fuzzy logic output, ΔD, can be obtained from the rule base Table-I.

The rule base is constructed using a fuzzy inference system (FIS), as outlined in Table I. Mamdani's method is applied for fuzzy rule evaluation, employing the Max-Min approach for rule combination. For instance, if ΔP(X) is classified as Positive Big (PB) and ΔI(X) as Negative Big (NB), then the output ΔD(X) is also Positive Big (PB). This implies that when the operating point is far from the MPP, the DC reference voltage (V_dc-ref) should be significantly increased to move the system toward optimal power extraction.

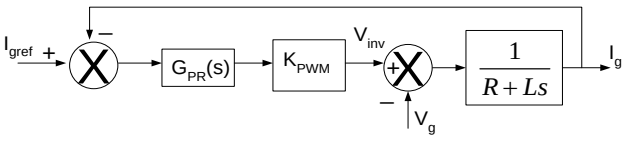

(a) the current controller

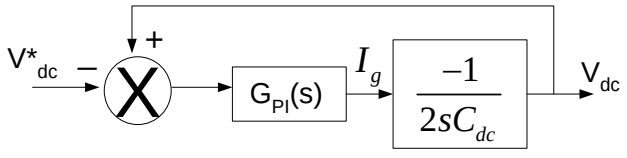

(b) the voltage controller

Fig. 5. Schematic representation

Defuzzification is the final stage of FLC, where linguistic variables are converted back into numerical values. In this process, the center of the area (COA) method is employed to translate the fuzzy subset memberships—representing variations in the DC voltage reference—into precise numerical values for implementation.

IARJSET ISSN (O) 2393-8021, ISSN (P) 2394-1588

International Advanced Research Journal in Science, Engineering and Technology

Impact Factor 8.066 ⁜ Peer-reviewed / Refereed journal ⁜ Vol. 12, Issue 2, February 2025

DOI: 10.17148/IARJSET.2025.12240

$$\Delta V_{dc-ref} = \frac{\sum_{i}^{N} \mu\left(V_{dc-ref,i}\right) V_{dc-ref,i}}{\sum_{i}^{N} \mu\left(V_{dc-ref,i}\right)} \quad (4)$$

3.2. CURRENT CONTROL SCHEME

Typically, the current controller's dynamic response is faster than the voltage controller. Therefore, the controller design primarily considers time delays and dynamic performance. Fig. 5(a) presents the schematic diagram of an internal-loop current controller, where the current reference signal I_{g_ref} and actual grid current I_g are compared to generate the error signal. The error signal is processed through a proportional-resonant (PR) controller to minimize deviations.

The PR controller offers several advantages, including fast dynamic response, low THD, maintaining sinusoidal grid current, effective disturbance rejection, and unity power factor operation. According to IEEE 929 standards, the current THD of the grid-tie inverter must not exceed 5%, while the individual limits for each odd harmonic (3^{rd} to 9^{th}) should remain below 4% [27-28]. Achieving these standards requires a well-designed current controller.

The PR controller transfer function used in the internal loop can be expressed as:

$$G_{PR}(s) = k_p + \frac{sk_i}{s^2 + \omega^2} \quad (5)$$

Where k_i and K_p represent the resonant and proportional gains, respectively, while, ω denotes the resonant frequency. To mitigate stability issues associated with an ideal PR controller, which exhibits infinite gain, Eq. (5) can be reformulated as:

$$G_{PR}(s) = k_P + k_i \frac{2w_c s}{s^2 + 2w_c s + w_0^2} \quad (6)$$

Where ω_c is the bandwidth around grid frequency.

The transfer function of current controller expressed as:

$$G_p(s) = \frac{I_g(s)}{V_{inv}(s)} = \frac{1}{R + Ls} \quad (7)$$

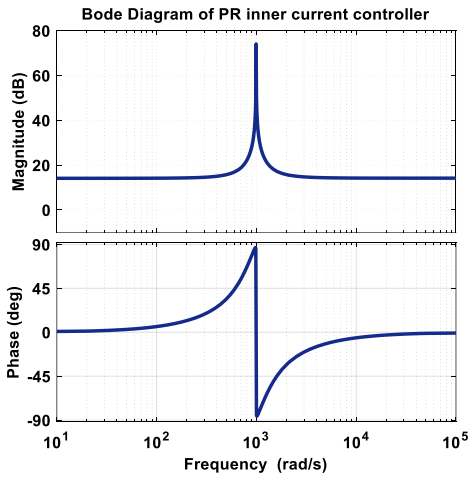

Fig. 6. PR controller Bode plot.

The gains of the PR controller are designed at bandwidth ω_c of 0.5rad/sec and resonant frequency (ω_o) of 314.15rad/s, obtaining a K_P = 2.55 and K_i = 1036.575. The Fig.6. shows the PR controller Bode plot Fig. 6.

3.3. Voltage Control Scheme

The DC link voltage is regulated by the voltage controller (VC). the reference signal V_{dc_ref} generated by the MPPT algorithm [29]. Fig. 5(b) illustrates the schematic diagram of the voltage controller. An error signal is generated by comparing actual DC voltage (V_{dc}) with reference (V_{dc_ref}), and a PI controller is used to minimize steady-state error.

IARJSET ISSN (O) 2393-8021, ISSN (P) 2394-1588

International Advanced Research Journal in Science, Engineering and Technology

Impact Factor 8.066 ⁜ Peer-reviewed / Refereed journal ⁜ Vol. 12, Issue 2, February 2025

DOI: 10.17148/IARJSET.2025.12240

The output of VC is the amplitude of current reference, and multiplied it by the sinusoidal unit derived from PLL to generate the actual grid reference current I_{g_ref} [30].

The external loop PI controller is designed with a low crossover frequency (typically between 5-20 Hz) to effectively attenuate the 100 Hz feedback from the DC link. The transfer function of voltage controller is:

$$G_{PI} = k_p + \frac{k_i}{s} \qquad (7)$$

Where K_P and K_I are current gains. The gains values are K_p = 0.01, K_I = 0.5, at 20 Hz crossover frequency. The transfer function in [31] is used here for completeness.

$$G_p(s) = \frac{V_{dc}(s)}{I_g(s)} = -\frac{1}{2sC_{dc}} \qquad (8)$$

The voltage controller is designed to attain a slower settling time, while the current controller could have a fast dynamic response meanwhile its main aims are stability and ideal regulation. Hence, the current controller must be decoupled and maintain the measured grid current could be considered equal to its grid current reference once design the voltage controller.

3.4. Douple Line Frequency (100Hz) Mitigation

When the utility grid's demand exceeds PV generation, the DC link capacitor discharges; when demand is lower, it charges. This causes a 100 Hz ripple, which requires proper capacitor design for effective filtering [30]. The DC link capacitor C_{dc} is calculated as:

$$\frac{d}{dt}\left(\frac{1}{2}CV_{dc}^2\right) = P_{pv} + P \qquad (9)$$

$$\frac{1}{2}C_{dc}\left(V_{dc\max}^2 - V_{dc\min}^2\right) = \int_{-T/8}^{T/8}\left(P_{PV} - P\right)dt \qquad (10)$$

From eq (10), the value of C_{dc} required to limit the ripple voltage is given in eq (11).

$$C_{dc} = \frac{P_{PV}}{2\omega.V_{dc}.\Delta V_{dc}} \qquad (11)$$

Where, $V_{dc} = \left(V_{dc\max}^2 + V_{dc\min}^2\right)/2$ and $\Delta V_{dc} = \left(V_{dc\max}^2 - V_{dc\min}^2\right)$

at $V_{dc} = 400V$, and desired voltage ripple ΔV_{dc} is 5% , then the calculated value of C_{dc} is equal to $540\mu F$.

4. SINGLE-PHASE GRID SYNCHRONIZATION ALGORITHM

The grid synchronization algorithm is vital for controlling single-phase PV inverters and determining grid voltage parameters (frequency, phase, amplitude) to detect deviations. Various algorithms have been studied and developed [32-33]. These methods can be classified as: 1) based on Fourier analysis, and 2) based on PLL technique [33].

Recently, PLL-based synchronization algorithms have garnered more attention due to their effectiveness. A transport-delay-based PLL offers a simple approach for implementing an orthogonal signal generator (OSG). Various techniques have been employed to generate the orthogonal signal, including PLL based on inverse Park transformation and Hilbert transformation. However, all of these PLL methods share certain characteristics and limitations, which are important to consider for optimal grid synchronization.

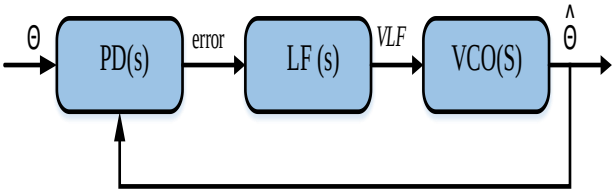

Fig. 7. Basic scheme of the PLL.

IARJSET ISSN (O) 2393-8021, ISSN (P) 2394-1588

International Advanced Research Journal in Science, Engineering and Technology

Impact Factor 8.066 ⁜ Peer-reviewed / Refereed journal ⁜ Vol. 12, Issue 2, February 2025

DOI: 10.17148/IARJSET.2025.12240

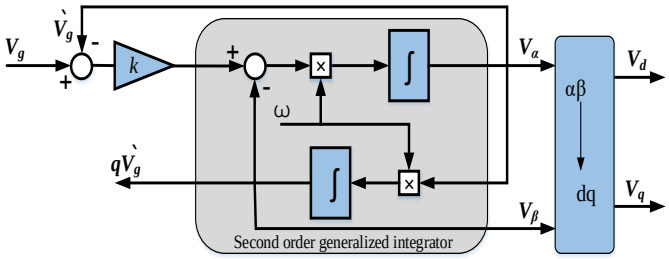

Fig. 8. PLL based on SOGI Schematic.

These techniques have certain drawbacks, such as nonlinearity, frequency dependence, and complexity, as outlined in [13]. To overcome these limitations, this article proposes a second-order generalized integrator (SOGI)-based PLL for orthogonal signal generation, providing an alternative to conventional PLL methods [31-33].

The basic PLL structure with SOGI is illustrated in Fig. 7 [27]. It consists of a loop filter (LF), a phase detector (PD), and a voltage-controlled oscillator (VCO). The small signal model for this PLL configuration is detailed in [31].

$$\frac{\hat{\Theta}(s)}{\Theta(s)} = \frac{k_p s + k_i}{s^2 + k_p s + k_i} \tag{12}$$

Where $\Theta(s)$, and $\hat{\Theta}(s)$ are respectively input and output phase angle, k_P and K_i are gains of the PLL.

A schematic of the PLL based SOGI is shown in Fig. 8. This PLL transfer functions expressed as:

$$G_{SOGI}(S) = \frac{\omega' s}{s^2 + \omega'^2} \tag{13}$$

$$G_d(S) = \frac{V_g'(s)}{V_g(s)} = \frac{k\omega' s}{s^2 + k\omega'^2 + \omega'^2} \tag{14}$$

$$G_q(S) = \frac{qV_g'(s)}{V_g(s)} = \frac{k\omega' s}{s^2 + k\omega'^2 + \omega'^2} \tag{15}$$

It is evident from eq (14) and (15), that the SOGI bandwidth depends on the gain *k*, and is independent of the center frequency ω, this characteristic makes the SOGI-based PLL technique suitable. The closed-loop gain is taken to 0.7.

5. DESIGN OF A LCL FILTER

The filter is required to mitigate the of PV inverter harmonics before injecting power into the grid [34-35] shown in Fig. 1. The configuration consists of inverter-side inductor (L_f). L_g and C_f are the grid-side connected inductor, and filter capacitor respectively. The current harmonic attenuation can be analyzed by considering inverter modeling as a harmonic generator and the grid is taken as a short circuit. LCL filter design considers inverter power, line frequency, and switching frequency, with values expressed as percentages of base values [35].

The calculation of base capacitor and impedance are as follows:

$$Z_b = V_r^2 / P_r, C_b = 1 / \omega_g \times Z_b \tag{16}$$

Where P_r is rated power (W), V_r is rated voltage (RMS), and ω_g is grid frequency.

For unipolar SPWM, the inverter-side inductor value is calculated by:

$$L_c = \frac{V_{dc}}{8 \times \Delta i_{fc\,max} \times f_s} \tag{17}$$

Where Δi_{fc} is the current ripple, f_s is the switching frequency. The accepted current ripple is calculated as:

$$\Delta i_{lf\,max} = \text{ripples}\% \times \frac{P_r \sqrt{2}}{V_r} \tag{18}$$

The filter capacitor is calculated by (19)

$$C_f = x.C_b \tag{19}$$

Where x is requirement of reactive power in percentage (x is taken 5%).

The L_g is calculated by [28].

$$\frac{f_s}{2} > f_r > \frac{f_s}{4} \tag{20}$$

IARJSET ISSN (O) 2393-8021, ISSN (P) 2394-1588

International Advanced Research Journal in Science, Engineering and Technology

Impact Factor 8.066 ⁜ Peer-reviewed / Refereed journal ⁜ Vol. 12, Issue 2, February 2025

DOI: 10.17148/IARJSET.2025.12240

$$L_{fg} = \frac{L_{fc}}{\left(\omega_r^2 \times L_{fc} \times C_f\right) - 1} \quad (21)$$

The aforementioned design procedure of LCL filter has been applied at rated power P_r = 2.7 kw, rated voltage V_r = 230V (RMS), switching frequency f_s = 10 kHz, and dc-link voltage V_{dc} = 400V the filter component values are calculated and given in Table II.

6. SIMULATION RESULTS AND DISCUSSIONS

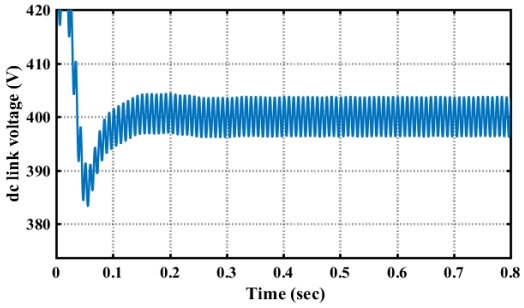

(a) Voltage at dc link

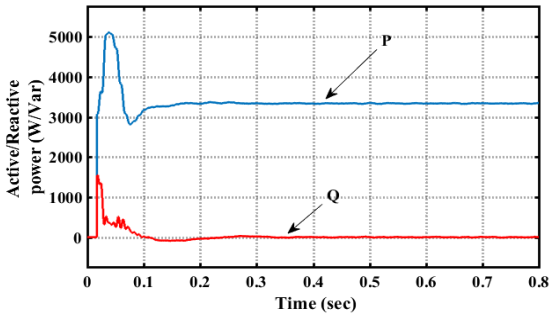

(b) Power devilever active/reactive

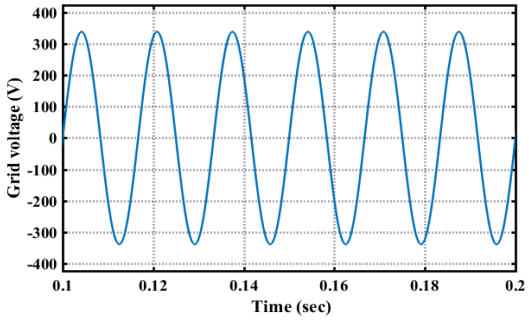

(c) Voltage at grid side

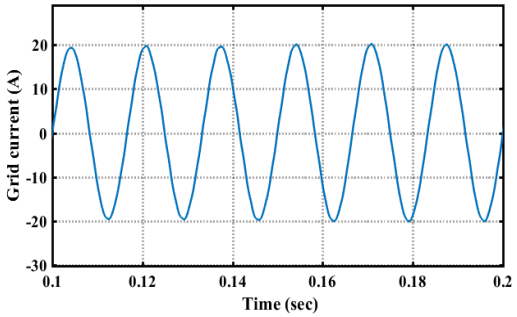

(d) Current at grid side

IARJSET ISSN (O) 2393-8021, ISSN (P) 2394-1588

International Advanced Research Journal in Science, Engineering and Technology

Impact Factor 8.066 ⁜ Peer-reviewed / Refereed journal ⁜ Vol. 12, Issue 2, February 2025

DOI: 10.17148/IARJSET.2025.12240

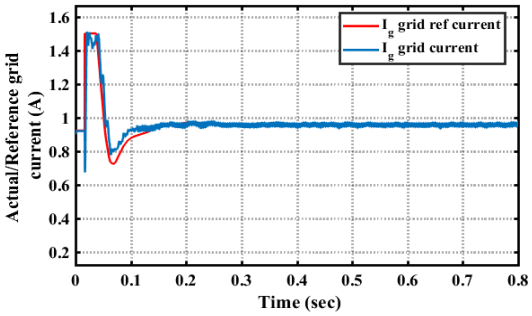

(e) actual/reference grid current.

Fig. 9. Simulation results

TABLE II SIMULATION PARAMETERS

DC-link voltage	V_{dc} = 400 V
Dc-link capacitor	C_{dc} = 540 µF
PV rated power	3.2 kW
Inverter switching frequency	f_s = 10 KHz
LCL filter	L_f =4.2mH,C_f=3µF,L_f
Grid nominal frequency	=2mH
Grid nominal vltage (RMS)	f_g = 60 Hz
	V_g = 230 V

Fig. 9 presents the proposed system simulation results at 1000 W/m², 25°C. The voltage of DC link is regulated effectively by the voltage controller within a short period (t = 0.1 sec) with minimal oscillations, (ref. Fig. 9(a)). The maximum power extraction by FLC-MPPT controller is shown in Fig. 10(b). Fig 9(c) and 9(d) display the waveform of the grid current and voltage, and they are in phase. hence, the reactive power shown in Fig.9(b) is zero. The comparison of actual and reference grid current generated by voltage controller output is shown in Fig. 9(e).

The FFT plot in Fig. 10 shows low grid current harmonics, meeting IEEE standards. Hence, the proposed methodology effectively maintains unity power factor during injection of maximum solar-PV power to the grid. Simulations were conducted under varying atmospheric conditions to verify the system's performance further. Initially, the surface temperature was maintained at 25°C while solar irradiance was varied from 1000 W/m² to 500 W/m², as depicted in Fig. 11(a). The Fig. 11(b) shows that the MPPT and DC link voltage controller respond promptly to the step change in solar irradiance, with minimal steady-state oscillation.

Fig. 11(c) shows that the DC link voltage controller regulates the grid current reference, which follows the actual grid current after a transient. A step change in solar irradiance at 0.6 sec reduces active power from 3.2 kW to 1.6 kW, while reactive power remains near zero. Fig. 11(d). Fig. 11(e) and 11(f) show the voltage and injected current into the grid. The grid current stays in phase with the voltage, maintaining THD below 5%, meeting IEEE 519 standards.

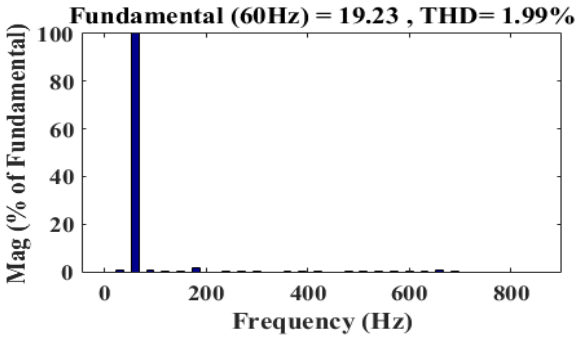

Fig. 10. THD of grid current.

IARJSET ISSN (O) 2393-8021, ISSN (P) 2394-1588

International Advanced Research Journal in Science, Engineering and Technology

Impact Factor 8.066 ⁜ Peer-reviewed / Refereed journal ⁜ Vol. 12, Issue 2, February 2025

DOI: 10.17148/IARJSET.2025.12240

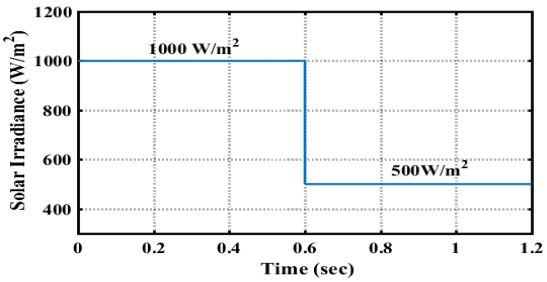

(a) Irradiance level

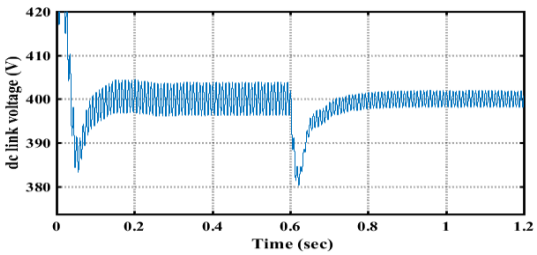

(b) Voltage across DC link

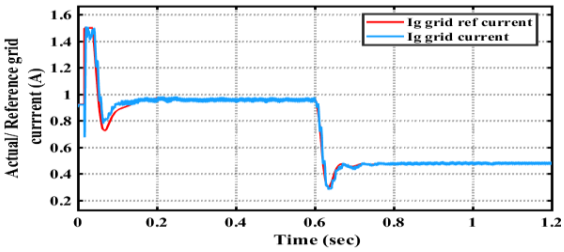

(c) Actual/ reference grid current

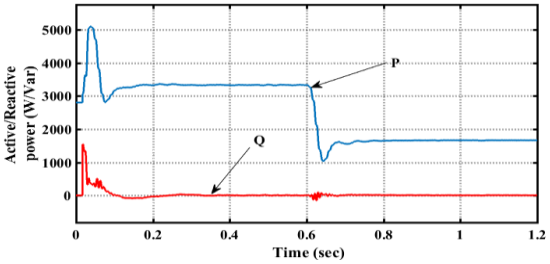

(d) Power active/ reactive

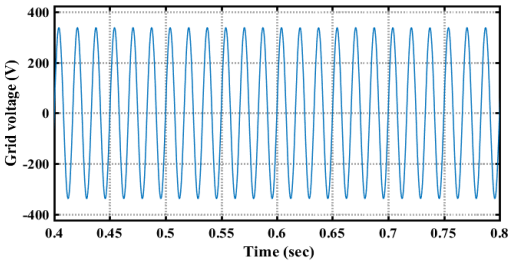

(e) grid voltage

IARJSET ISSN (O) 2393-8021, ISSN (P) 2394-1588

International Advanced Research Journal in Science, Engineering and Technology

Impact Factor 8.066 ⁜ Peer-reviewed / Refereed journal ⁜ Vol. 12, Issue 2, February 2025

DOI: 10.17148/IARJSET.2025.12240

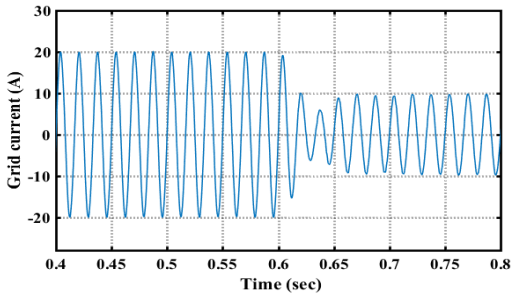

(f) grid current

Fig. 11. System responses at variations of solar irradiance level

7. CONCLUSION

This paper presents a grid-connected, single-phase, single-stage PV power system with an efficient control approach for enhanced performance and grid compliance. The system integrates a fuzzy logic-based MPPT algorithm to maximize power extraction, a DC-link voltage regulator for stability, and a current controller to ensure high-quality power injection. The MPPT controller effectively adjusts to varying atmospheric conditions, while the desired DC-level is achieved by the voltage controller. Simulation results exhibited the proposed control strategy is perform effectively, by injecting low THD (1.99%) sinusoidal current into the grid, meeting IEEE 519 standards. Additionally, the system operates with a near-unity power factor, ensuring efficient energy transfer.

REFERENCES

[1] A K Maurya and Yogesh K Chauhan, "Performance of Isolated Generating System with Multilevel Inverter using Photovoltaic Source," IEEE International Conference AICERA:ICMiCR 2013. pp.1-6, Jun 2013. DOI: 10.1109/AICERA-ICMiCR.2013.6576004

[2] K. Chahar, A K Maurya and A. Chaturvedi, "Performance analysis of fuel cell assisted distributed generation system," IEEE International Conference on Contemporary Computing and Informatics (IC3I), pp. 426-429, Nov. 2014. DOI: 10.1109/IC3I.2014.7019604

[3] A K Maurya, S.P. Singh, and Y V Hote, "Direct Drive Ocean Wave Energy Converter Based Off-grid Supply System" IEEE 10th Power India International Conference (PIICON 2022), New Delhi, pp. 1-6, Nov. 2022. DOI: 10.1109/PIICON56320.2022.10045182.

[4] A K Maurya and S.P. Singh, "A study on ocean wave power and utilization for Indian coastal region" IEEE Asian Conf. on Energy, Power and Transportation Electrification (ACEPT), Singapore, pp. 1-9, 2017. DOI: 10.1109/ACEPT.2017.8168544.

[5] S.K. Das, A K Maurya, S. Sisodiya and P. Raghuwanshi (2024). Book title: Spark of Change: Revolutionizing Transportation with EVs. ISBN: 9789362523822, IIP Publisher.

[6] A K Maurya & S. P. Singh, "Analysis of Buck-Boost Inverter Installed in Permanent Magnet Linear Generator-based Ocean Wave Energy Converter," Taylor & Francis, IETE Journal of Research, Vol. 70, no.1, pp. 862-874, 2022. https://doi.org/10.1080/03772063.2022.2112311

[7] A K Maurya and S.P. Singh, "Analysis of Cascaded Buck-Boost Inverter for PMLG based Ocean Wave Energy Converter," Taylor & Francis, IETE Journal of Research, Vol.68, no.6, pp. 4109-4119, 2020. https://doi.org/10.1080/03772063.2020.1787874

[8] A K Maurya and S.P. Singh, "Assessment of Ocean Wave Energy Converters for Indian Coastal region," Taylor & Francis, IETE Technical Review, vol. 32, no. 5, pp. 476-488, 2019. https://doi.org/10.1080/02564602.2019.1659189

[9] A K Maurya, Y. K Chauhan and R. K. Mishra, "Fuel Cell Integrated with Five Level VSI for Industrial Pump Applications," International Journal of Renewable Energy Research (IJRER), Vol. 3, no.2, pp. 388-394, 2013. https://doi.org/10.20508/ijrer.v3i2.618.g6154

[10] A K Maurya, K Chahar, and Y. K. Chauhan," Analysis on Photovoltaic Assisted Three Phase five level Unipolar PWM Inverter for Induction Motor Driven Water Pumping System" ACCENTS International Journal of Advanced Computer Research, Vol. 3, no.1, pp. 31-35, 2013.

[11] A K Maurya and Y K Chauhan, "Multilevel Converter-Photovoltaic Source Based Single-phase Standalone Generating System," IEEE International Conference on Energy Efficient Technologies for Sustainability (ICEETS'13), pp. 943 – 948, 10-12 April 2013. DOI: 10.1109/ICEETS.2013.6533514

[12] Bo Yang, Wuhua Li, Yi Zhao, and Xiangning He, "Design and Analysis of a Grid-Connected Photovoltaic Power System," *IEEE Trans. Power Electron*, vol. 25, no. 4, pp. 992-1000. Apr 2010. doi: 10.1109/TPEL.2009.2036432.

DOI: 10.17148/IARJSET.2025.12240

[13] B. N. Alajmi, K. H. Ahmed, G. P. Adam, B. W. Williams, "Single-Phase Single-Stage Transformer Less Grid-Connected PV System," IEEE Trans. Power Electron, vo. 28, no. 6, pp. 2662-2676. Jun 2013. DOI: 10.1109/TPEL.2012.2228280.

[14] A. Alenezi and H. A. Hussain, "A New Control Approach for Least Processed Power Tracking Under Mismatch Conditions in PV Systems Using Differential Power Processing," in IEEE Transactions on Industry Applications, vol. 60, no. 1, pp. 532-543, Jan.-Feb. 2024, doi: 10.1109/TIA.2023.3312651

[15] F. E. Aamri et al., "Stability Analysis for DC-Link Voltage Controller Design in Single-Stage Single-Phase Grid-Connected PV Inverters," in IEEE Journal of Photovoltaics, vol. 13, no. 4, pp. 580-589, July 2023, doi: 10.1109/JPHOTOV.2023.3263253.

[16] K. Alluhaybi, I. Batarseh and H. Hu, "Comprehensive Review and Comparison of Single-Phase Grid-Tied Photovoltaic Microinverters," in IEEE Journal of Emerging and Selected Topics in Power Electronics, vol. 8, no. 2, pp. 1310-1329, June 2020, doi: 10.1109/JESTPE.2019.2900413.

[17] S. K. Kuncham, K. Annamalai and S. Nallamothu, "Single-Phase Two-Stage Seven-Level Power Conditioner for Photovoltaic Power Generation System," in IEEE Journal of Emerging and Selected Topics in Power Electronics, vol. 8, no. 1, pp. 794-804, March 2020, doi: 10.1109/JESTPE.2019.2913216.

[18] S. Dasgupta, S. K. Sahoo, S. K. Panda and G. A. J. Amaratunga, "Single-Phase Inverter-Control Techniques for Interfacing Renewable Energy Sources With Microgrid—Part II: Series-Connected Inverter Topology to Mitigate Voltage-Related Problems Along With Active Power Flow Control," in IEEE Transactions on Power Electronics, vol. 26, no. 3, pp. 732-746, March 2011, doi: 10.1109/TPEL.2010.2096590.

[19] P. K Pardhi, S K Sharma, and A Chandra, (2022) "Grid-integrated single phase solar PV system employed with single switch high gain boost converter", Elsevier journal of Electric Power Systems Research, Vol 213, pp. 1-13, https://doi.org/10.1016/j.epsr.2022.108231.

[20] Q. Zhong, Y. Qiu, Y. Zhao, H. Li, G. Wang and F. Wen, "Interharmonic Analysis Model of Photovoltaic Grid-connected System with Extended Dynamic Phasors," in *Journal of Modern Power Systems and Clean Energy*, vol. 9, no. 6, pp. 1540-1547, November 2021, doi: 10.35833/MPCE.2020.000241.

[21] B. N. Alajmi, K. H. Ahmed, S. J. Finney and B. W. Williams, "Fuzzy-Logic-Control Approach of a Modified Hill-Climbing Method for Maximum Power Point in Microgrid Standalone Photovoltaic System," in *IEEE Transactions on Power Electronics*, vol. 26, no. 4, pp. 1022-1030, April 2011, doi: 10.1109/TPEL.2010.2090903.

[22] N. Khaehintung, K. Pramotung, B. Tuvirat and P. Sirisuk, "RISC-microcontroller built-in fuzzy logic controller of maximum power point tracking for solar-powered light-flasher applications," *30th Annual Conference of IEEE Industrial Electronics Society, 2004. IECON 2004*, Busan, Korea (South), 2004, pp. 2673-2678 Vol. 3, doi: 10.1109/IECON.2004.1432228.

[23] A K Maurya and Y K Chauhan, "Application of Generalized Instantaneous Reactive Power Theory for Three-Phase Four-Wire System," International Journal of Engineering and Technology, Vol.4, no 6, pp. 372-359, 2013.

[24] Maurya, A.K., Chauhan, Y.K. (2013). Simplified Control Algorithm Based on IRP Theory for Three Phase Shunt Active Power Filter. In: Singh, K., Awasthi, A.K. (eds) Quality, Reliability, Security and Robustness in Heterogeneous Networks. QShine 2013. Lecture Notes of the Institute for Computer Sciences, Social Informatics and Telecommunications Engineering, vol 115. Springer, Berlin, Heidelberg. https://doi.org/10.1007/978-3-642-37949-9_37

[25] I Aggarwal and A K Maurya, "Performance Analysis of NEURO-FUZZY based Power Conditioner," International Journal of Engineering and Technology, Vol.5, no 2, pp. 686-691, 2013

[26] IEEE Recommended Practice and Requirements for Harmonic Control in Electric Power Systems, in IEEE Std 519-2014 (Revision of IEEE Std 519-1992) , vol., no., pp.1-29, 11 June 2014, doi: 10.1109/IEEESTD.2014.6826459.

[27] Characteristics of the Utility Interface for Photovoltaic (PV) Systems, IEC 61727 CDV (Committee Draft for Vote), 2002.

[28] "IEEE Standard for Interconnecting Distributed Resources with Electric Power Systems," in IEEE Std 1547-2003 , vol., no., pp.1-28, 28 July 2003, doi: 10.1109/IEEESTD.2003.94285.

[29] E. Villanueva, P. Correa, J. Rodriguez and M. Pacas, "Control of a Single-Phase Cascaded H-Bridge Multilevel Inverter for Grid-Connected Photovoltaic Systems," in *IEEE Transactions on Industrial Electronics*, vol. 56, no. 11, pp. 4399-4406, Nov. 2009, doi: 10.1109/TIE.2009.2029579.

[30] N. Vázquez, J. Vázquez, J. Váquero, C. Hernández, E. Vázquez and R. Osorio, "Integrating Two Stages as a Common-Mode Transformerless Photovoltaic Converter," in *IEEE Transactions on Industrial Electronics*, vol. 64, no. 9, pp. 7498-7507, Sept. 2017, doi: 10.1109/TIE.2017.2682014.

[31] V. N. Lal and S. N. Singh, "Control and Performance Analysis of a Single-Stage Utility-Scale Grid-Connected PV System," in *IEEE Systems Journal*, vol. 11, no. 3, pp. 1601-1611, Sept. 2017, doi: 10.1109/JSYST.2015.2408055.

[32] Y. Yang, F. Blaabjerg and Z. Zou, "Benchmarking of grid fault modes in single-phase grid-connected photovoltaic systems," *2012 IEEE Energy Conversion Congress and Exposition (ECCE)*, Raleigh, NC, USA, 2012, pp. 4370-4377, doi: 10.1109/ECCE.2012.6342228.

IARJSET ISSN (O) 2393-8021, ISSN (P) 2394-1588

International Advanced Research Journal in Science, Engineering and Technology

Impact Factor 8.066 ⁜ Peer-reviewed / Refereed journal ⁜ Vol. 12, Issue 2, February 2025

DOI: 10.17148/IARJSET.2025.12240

[33] R. Teodorescu, M. Liserre, and P. Rodriguez, *Grid Converters for Photovoltaic and Wind Power Systems*. Hoboken, NJ, USA: Wiley, 2011.

[34] J. Dannehl, C. Wessels and F. W. Fuchs, "Limitations of Voltage-Oriented PI Current Control of Grid-Connected PWM Rectifiers With *LCL* Filters," in *IEEE Transactions on Industrial Electronics*, vol. 56, no. 2, pp. 380-388, Feb. 2009, doi: 10.1109/TIE.2008.2008774.

[35] M. Liserre, F. Blaabjerg and S. Hansen, "Design and control of an LCL-filter-based three-phase active rectifier," in *IEEE Transactions on Industry Applications*, vol. 41, no. 5, pp. 1281-1291, Sept.-Oct. 2005, doi: 10.1109/TIA.2005.853373.